Luminescence mechanisms in 6H-SiC nanocrystals

J. Botsoa,[1] J. M. Bluet,[1] V. Lysenko,[1] L. Sfaxi,[2] Y. Zakharko,[1] O. Marty,[3] and G. Guillot[1]
[1]*Institut des Nanotechnologies de Lyon (INL), CNRS UMR 5270, INSA de Lyon, Villeurbanne F-69621, France*
[2]*Laboratoire de Physique des Semiconducteurs et des Composants Electroniques, Faculté des Sciences de Monastir, Avenue de l'Environnement, 5000 Monastir, Tunisia*
[3]*Institut des Nanotechnologies de Lyon (INL), CNRS UMR 5270, Université de Lyon 1, Villeurbanne F-69622, France*
(Received 26 March 2009; revised manuscript received 16 July 2009; published 15 October 2009)

Experimental conditions allowing consequent selection of a dominating photoluminescence mechanism in 6H-SiC nanocrystals at room temperature are reported. Electrostatic screening of surface states involved in radiative transitions can be efficiently achieved by polar ethanol molecules. This leads to a preponderant radiative channel between the electronic levels corresponding to the impurity atoms (N and Al). This radiative channel is deactivated by centrifugation-induced selection of the smallest colloidal 6H-SiC nanocrystals in which the probability to have both donor and acceptor atoms is negligible. Consequently, for these smallest 6H-SiC nanocrystals with switched off transitions between surface states and impurity levels, quantum-confinement effect can be clearly observed. The formation of energy subbands in the 6H-SiC nanocrystals is then evidenced from photoluminescence excitation and absorption measurements performed on the centrifuged colloidal nanosuspension. A most probable mean diameter of 1.9 nm for these particles is deduced from calculation of energy levels in the effective-mass approximation.

DOI: 10.1103/PhysRevB.80.155317 PACS number(s): 78.67.Bf, 78.55.Qr

I. INTRODUCTION

Nanostructured silicon carbide (SiC) has generated a surge of scientific interest in recent years due to its potentialities in optoelectronics as an efficient ultraviolet (UV) emitter. Yet, the amount of theoretical and experimental works devoted to the understanding of the mechanisms involved in the photoinduced light-emission process in this material is much smaller than that devoted to nanostructured Si. Photoluminescence (PL) studies performed so far on nanostructured SiC have been carried out mainly at room temperature on porous SiC (PSC) nanostructures obtained by electrochemical anodization etching.[1–6] Radiative recombinations via surface states and impurity levels have been discussed in literature as the main mechanisms for the observed PL signals coming from the PSC nanostructures.[1–5] However, the results of these PL measurements were disappointing with respect to an expected above-gap UV emission due to quantum confinement. For instance, in the case of porous 6H-SiC, only a broad subband-gap PL peak (in the blue-green spectral range) was generally observed.[6] A comparative study carried out by Konstantinov *et al.*[2] showed that the PL spectra of porous 3C-, 4H-, and 6H-SiC are similar even though the band-gap energies of the initial bulk substrates differ by up to 0.9 eV. The authors suggested that the photoluminescence in these nanostructures is rather associated with surface states. It is only a few years ago that a clear evidence of quantum confinement in colloidal 3C-SiC nanocrystals has been reported.[7–9] The main argument for confinement quantum-effect observation in Ref. 7 is the blueshift of the above band-gap photoluminescence peak when the excitation source energy is enhanced interpreted as a consequence of nanoparticles size distribution. Similar to previous studies on Si nanostructures, two luminescence mechanisms were proposed for the SiC nanostructures: band-to-band radiative transitions between confined photogenerated carriers and radiative transitions via surface states.

In this paper we show that both mechanisms are indeed present. Furthermore, we describe how one can manage these different competitive radiative channels in the PL of 6H-SiC nanocrystals. In particular, we show that the PL mechanisms related to radiative transitions via surface and impurity levels in the 6H-SiC nanocrystals can be "switched off" allowing clear manifestation of quantum confinement with observation of energy subbands in the nanocrystals. We then tackle an important question concerning the photoluminescence of SiC nanostructures: why was quantum-confinement effect not clearly observed up to now in nanoporous SiC while it has been in 3C-SiC nanocrystal suspension?

II. EXPERIMENT

Strongly interconnected 6H-SiC nanocrystals forming a porous network were obtained by electrochemical anodization etching of a 0.054 Ω cm *n*-type bulk 6H-SiC wafer. Capacitance vs voltage measurements on the wafer using an Hg probe allowed us to determine a donor (nitrogen) concentration of 2×10^{18} at cm^{-3} while a small compensation by aluminum (10^{16} at cm^{-3}) has been measured by secondary-ion mass spectroscopy. The etching process took place for 25 min under UV illumination on the carbon face of the 6H-SiC wafer at a current density of 270 mA/cm^2. A 1:1 in volume mixture of HF(50%)/ethanol was used as electrolyte. At the end of the porosification regime, a short high-current monopulse (1.0 A/cm^2) was applied to remove the formed porous layer from the wafer. A mechanical grinding in an agate mortar of the formed nanoporous free layer allowed us to obtain a SiC nanopowder consisting of numerous separated nanoparticles.

PL measurements were performed using a laser line at 244 nm from a frequency-doubled Ar^+ laser for the excitation. The light dispersion and detection were obtained using

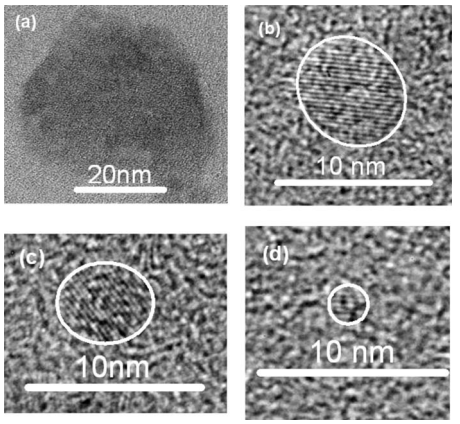

FIG. 1. Several examples of highly resolved TEM images of the nanoparticles constituting the initial 6H-SiC nanopowder.

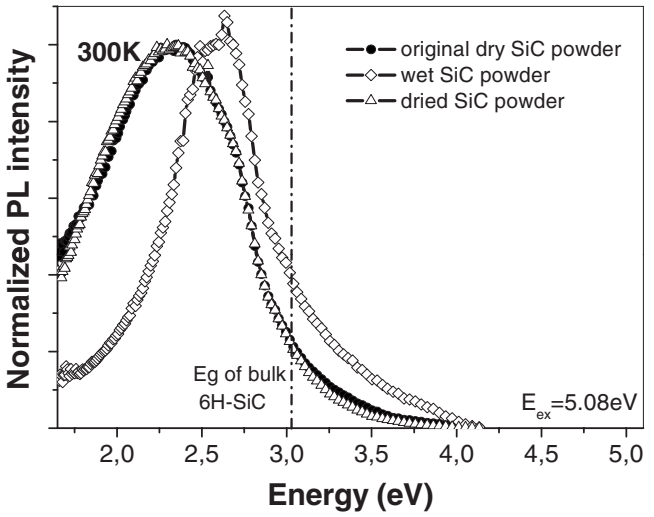

FIG. 2. Room-temperature PL spectra of original dry, wetted, and dried (after ethanol evaporation) SiC nanopowder. Spectra are normalized to the maximum intensity of the wetted nanopowder.

a spectrometer (Jobin-Yvon HRS-2) and a GaAs cathode photomultiplier (Hamamatsu H5701–50), respectively. Measured PL spectra were corrected with respect to the spectral response of the whole optical system. PL and PLE (photoluminescence excitation) measurements of colloidal nanoparticles were performed using a PTI spectrofluorometer working in a right-angle scattering geometry equipped with a 75 W xenon arc lamp as excitation source, an excitation and emission monochromator for excitation and emission wavelength selection, and a photomultiplier tube for detection. Absorption measurements were performed in quartz cuvettes using a UV-visible Perkin Elmer spectrophotometer. The net nanoparticles absorption was obtained by subtracting the cuvette+ethanol response.

III. RESULTS AND DISCUSSION

A. Transmission electron microscopy

The nanopowder dispersed on a graphite grid was observed by means of transmission electron microscopy (TEM). Several examples of the most typical nanoparticles constituting the nanopowder are shown in Fig. 1. They indicate a relatively large initial size distribution of the nanoparticles. Indeed, both large (>10 nm) and smaller nanoparticles (<10 nm) can be observed. Large nanoparticles consist of interconnected smaller nanoparticles not separated during the grinding. The crystalline small nanoparticles have sizes ranging from 10 nm down to 1.8 nm in diameter for the smallest ones. The measured atomic plane distance of 0.25 nm corresponds with the compact plane spacing in SiC polytype. No oxide shell surrounding the particles was observed. The absence of this oxide shell has been confirmed by infrared spectroscopy measurements performed by Alekseev *et al.*[10] on the nanoporous SiC layer.

B. Influence of ethanol solvent on the PL of 6H-SiC nanoparticles

In order to bring to the fore the important role of surface states in the PL of these nanoparticles, the chemical environment of the nanoparticles has to be varied. Room-temperature PL measurements using the 244 nm laser line were performed at the following three stages: (i) when the SiC nanopowder was initially dry, (ii) shortly after the nanopowder was wetted with ethanol and later, and (iii) when the ethanol has been completely evaporated. The normalized recorded spectra are given in Fig. 2. One can clearly see that the PL spectrum of the wetted SiC nanopowder is blueshifted and narrowed in comparison to that of the dry nanopowder. For the wetted nanopowder, the PL peak centered at 2.65 eV corresponds to N-Al donor-acceptor-pair (DAP) recombination commonly observed in bulk 6H-SiC substrates.[11] This N-Al DAP band was besides measured on the starting material.[12] For the dry nanopowder, the PL signal centered at 2.3 eV is different from the PL spectra detected on the bulk material. Furthermore, the above-gap tail in the PL spectrum is more pronounced for the wetted powder. The coincidence of the spectrum of the initially dry nanopowder and that of the nanopowder after evaporation of ethanol demonstrates the completely reversible interaction between ethanol and the nanoparticles. It is also important to mention that the integrated PL intensity (calculated over the energy spectral range from 1.6 to 4.25 eV) of the wet nanopowder is five times higher than the integrated PL intensity of the dry powders.

In Ref. 8, Fan *et al.* argues that the solvent (water, toluene, or ethanol) keeps individual 3C-SiC particles apart and provides a high potential barrier for electrons and holes ensuring quantum confinement. In their case, the luminescence comparison is made between the nanoporous structure with interconnected crystallites and the nanoparticles dispersed in the different solvents. Indeed, in this case, the role of the solvent is mainly to disperse the nanoparticles and to prevent the transfer of photoexcited carriers from small nanoparticles to larger ones where they can recombine.[12] The comparison illustrated by Fig. 2 is different because in the dry powder the nanoparticles are not interconnected contrary to the nanoporous network. Consequently, the solvent wetting effect shown in Fig. 2 is not only due to dispersion of the nanoparticles. As it is completely reversible, this effect is also not

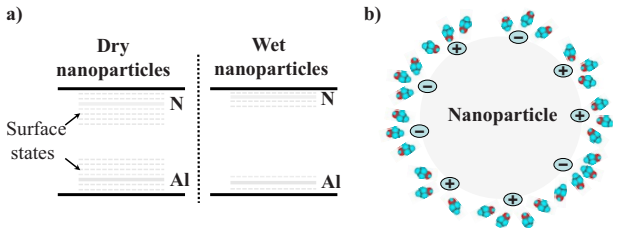

FIG. 3. (Color online) Schematic representation of (a) far-field and (b) near-field interaction of a highly dielectric solvent with the nanoparticles. Evolution of the energy-band diagram of the nanoparticles upon ethanol wetting is shown in part (a). Due to the far-field dielectric screening effect, the energy levels of surface states and, to a less extent, impurity atoms (N and Al) move toward the band edges. The energy distribution of the surface and defect states inside the band gap is considerably narrowed. Local dipolar interaction of polar molecules with charged surface states of the nanoparticle are illustrated in part (b).

due to any chemical reaction leading to the surface passivation of the nanoparticles.

To explain this solvent wetting effect, both radiative and nonradiative surface states will be considered. First of all, it should be stated that the general origin of electronically active (donorlike or acceptorlike) surface states can be related to different local defect sites (dangling bonds, numerous structural defects, etc.) appearing in excess at the surface of the SiC nanoparticles obtained by a relatively aggressive electrochemical etching of the bulk crystalline SiC. Thus, the observed PL behavior of the 6H-SiC nanopowder caused by ethanol (Fig. 2) can be explained first by an efficient far-field electrostatic screening of both nonradiative and radiative surface states. This dielectric effect is well known in porous Si nanostructures for which a blueshift of the photoluminescence was observed when the sample was wetted by a solvent[13] or embedded in a polymer.[14] Indeed, ethanol (or any other solvent with a static dielectric constant higher than that of SiC) induces a global increase in the effective dielectric function of the nanoparticle environment. Considering a hydrogenic impurity model, Timoshenko *et al.*[15] have shown that this higher effective dielectric constant of the medium (solvent+nanoparticles) leads to an important decrease in their energy depth inside the energy-band gap. This far-field dielectric effect is schematically represented in Fig. 3(a). A near-field electrostatic screening of the surface states at molecular level has also to be mentioned. Indeed, highly polar ethanol molecules are attracted to and form weak links (without creation of strong chemical bonds between the ethanol molecules and surface defects) with the surface charges of the nanoparticles [see schematic representation in Fig. 3(b)]. This near-field interaction leads (i) to an important local redistribution of the electrical charges at the nanoparticle-ethanol interface and even (ii) to a possible disappearance of some surface states from the electronic band gap of the 6H-SiC nanoparticles. We have to specify that this dielectric effect has a more important impact on the surface states than, for example, on the ionization energies of the impurities or defects situated deeper in the nanoparticle volume.

Within the frame of the near- and far-field dielectric effect described above, the PL intensity enhancement in the case of

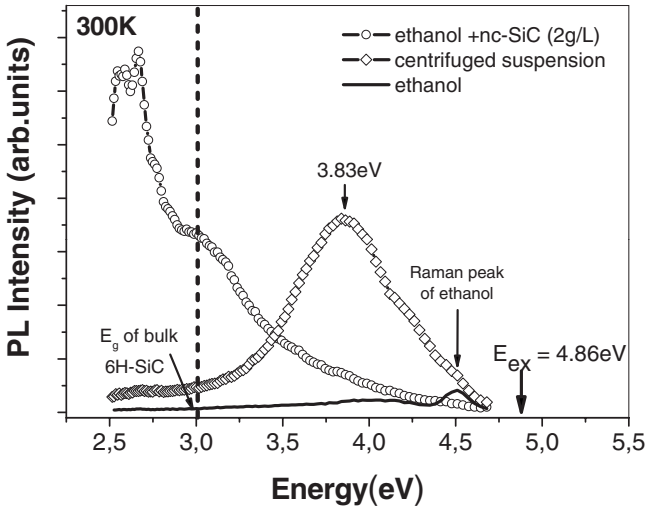

FIG. 4. Evolution of the PL spectrum of 6H-SiC nanocrystal suspensions induced by size selection of nanocrystals during centrifugation.

the wetted 6H-SiC nanopowder can be explained by the decrease in transitions via nonradiative surface recombination centers because (i) of the ethanol-induced displacement of their energy positions toward the band edges or (ii) of their disappearance from the energy-band gap. The dielectric effect influences in a similar manner the radiative surface centers being initially distributed over a large energy range inside the band gap and ensuring room-temperature PL emission of the nanoparticles in air with the 2.3 eV peak (Fig. 2). The modification of the surface states energy positions or their disappearance from the energy-band gap induced by ethanol wetting leads (i) to the observed narrowing of the whole PL spectrum as well as (ii) to the relative enhancement of other recombination channels role. These channels are radiative transitions between the donor-acceptor pairs (2.65 eV) dominating the spectrum of the wetted SiC nanopowder and radiative transitions linked to quantum confinement (emissions at energies higher than the band gap of bulk 6H-SiC, i.e., >3.0 eV).

C. Quantum-confinement effect: energy-subband observation

A simple estimation performed from the known concentration values of the impurity centers in the initial bulk 6H-SiC substrates shows that the probability of having both N and Al impurities in small nanocrystals exhibiting confinement quantum effect (<10 nm) is very low. Indeed, considering the Al concentration, an Al atom will be present only in nanoparticles with diameters higher than 14 nm. Therefore, the dominant PL peak at 2.65 eV corresponding to the radiative transitions between the N-Al donor-acceptor pairs in the wetted 6H-SiC nanopowder is rather due to light emission from large (with dimensions >30 nm) nanocrystals. To switch off this radiative transition between the impurities in the nanopowder, one should exclude the large nanoparticles from the suspension. To reach this goal we used a centrifugation. 12 successive centrifugations were carried out at

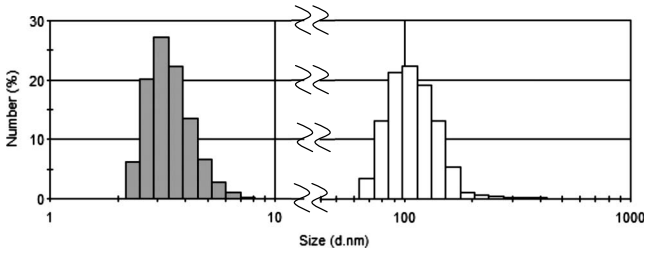

FIG. 5. Size distribution obtained from granulometry measurements. White distribution is for the as-prepared solution and the gray one after successive centrifugations.

$3000 \times g$ for 1 min on a suspension of 6H-SiC nanoparticles in ethanol.

Figure 4 shows the PL emissions detected from the nanoparticle suspensions prior to and after the last centrifugation treatment. In agreement with the previous results concerning ethanol-wetted 6H-SiC nanopowder, one can see that the initial 2 g/l suspension of the 6H-SiC nanoparticles gives a main PL emission around 2.65 eV and an above-gap component. The centrifuged colloidal suspension gives a single broad ultraviolet PL peak centered at 3.83 eV. Further centrifugation leaves the PL line shape and maximum energy unchanged. Hence, the 3.83 eV peak can be associated with the intrinsic luminescence from quantum-confined photogenerated carriers in the smallest 6H-SiC nanoparticles present in the suspension. Based on these observations, we can conclude that the centrifugation technique has efficiently allowed the separation of the smallest nanoparticles exhibiting quantum confinement from large ones in which radiative transitions between the impurity electronic states dominate. This expected effect of centrifugation has been confirmed by optical granulometry measurements on 3C-SiC nanoparticles suspension in ethanol obtained exactly in the same way that the 6H ones. In Fig. 5 is presented the initial size distribution and the one after successive centrifugations. One can clearly see the centrifugation efficiency to remove the bigger particles and to obtain a monomodal distribution of particles diameter centered at 2 nm.

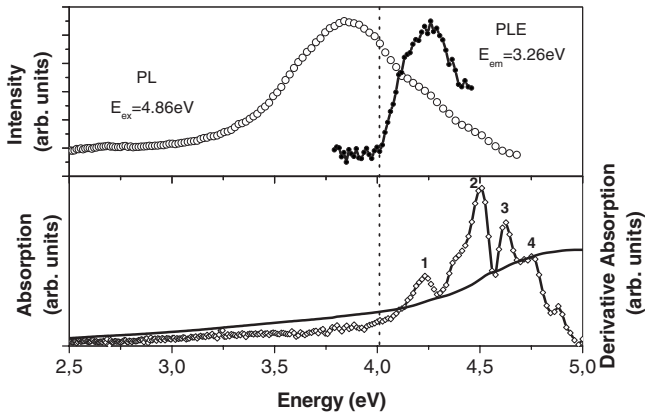

FIG. 6. Photoluminescence (PL in open circles), photoluminescence excitation (PLE in line+solid circles), absorption (in straight line), and derivative absorption (in line+open diamond) spectra of the final centrifuged suspension containing only the smallest 6H-SiC nanoparticles for which quantum confinement of the photoexcited carriers is clearly manifested.

Figure 6 gives us extra information on the electronic states of the smallest nanoparticles present in the final centrifuged suspension. In particular, photoluminescence, PLE, and absorption measurements were found to be strongly correlated. The PLE spectrum was obtained with an emission energy fixed at 3.26 eV. The absorption spectrum and its first derivative are shown in Fig. 6. The derivative is presented in order to emphasize the fine structuring observed in the absorption spectrum in the range of 4–5 eV. In particular, the peaks on the derivative absorption spectrum correspond to the steplike features on the continuously rising absorption spectrum. These peaks are numbered from 1 to 4. The threshold position (4 eV) for peak 1 corresponds to the threshold position of the PLE peak (dot line in Fig. 5). Thus, we have a Stokes shift of 170 meV between fundamental absorption and fluorescence which can originate from structural relaxation to a lower-energy configuration prior to emission (classical Franck-Condon shift) and also from solvent relaxation phenomena. Indeed, we consider that during the lifetime of the excited state, the lattice configuration of the nanoparticle relaxes to a new configuration of lower total energy leading to a redshift of luminescence with respect to absorption. Furthermore, in Si quantum dots the Franck-Condon shift can be as large as 60 meV for 2 nm dot due to splitting of the excited state in singlet and triplet states.[16] This can also be an explanation for the large shift observed here. Additionally to this, we have to consider the solvent relaxation effect. Indeed, the rearrangement of the solvent cage around the nanoparticle during the lifetime of the excited state may also increase the emission redshift.[17]

These observations, confirm that peak 1 corresponds to the fundamental confined level in 6H-SiC nanoparticles present in the centrifuged suspension. Notably, the threshold of peak 1 (4.0 eV) corresponds to the effective band gap of the nanoparticles which is clearly widened compared to its bulk value because of quantum confinement. A rapid estimation based on Brus model[18] enables us to determine that the corresponding size of these nanoparticles is around 2.0 nm. This corresponds well to the smallest nanoparticles observed in TEM (see Fig. 1). Peaks 2, 3, and 4 can thus be attributed to the excited states in these nanoparticles. These corresponding peaks cannot be observed on the PLE spectrum because of the spectral limitation of the fluorometer used. To check these assumptions, more thorough theoretical calculations were carried out.

We give here a brief description of the theoretical model which has been described in detail elsewhere.[19] In order to determine electron and hole energy levels and their wave functions, three-dimensional time-independent Schrödinger equation has been solved using the envelope-function formalism and the effective-mass approximation. The orthonormal wave-function expansion method was used. We consider spherical SiC dots embedded in a sphere of a barrier material and we assume the wave function as a linear combination of the expansion basis functions. The problem then becomes an eigenvalue problem of Hamiltonian matrix H_0. The matrix elements are evaluated from

TABLE I. Comparison of calculated and experimentally deduced values for fundamental and excited levels for a 1.9 nm in diameter 6H-SiC nanocrystal.

Energy levels	Values derived from the derivative absorption spectrum (eV)	Calculated values (eV)
Fundamental level	4.0	4.04
1st excited state	4.3	4.44
2nd excited state	4.6	4.61
3rd excited state	4.7	5.01

$$H_{nml,n'm'l'} = \int_{\Omega}\int\int\left[-\Psi^{*}_{nml}\left(\nabla\frac{\hbar^2}{2m^{*}}\nabla\right)\Psi_{n'm'l'} + \Psi_{nml'}V\Psi_{n'm'l'}\right]d\Omega, \quad (1)$$

where m^* is the position-dependent effective mass and V is the position-dependent potential, both assumed constant within the dot ($m^*=m^*_{\mathrm{dot}}$; $V=0$) and within the matrix ($m^*=m^*_{\mathrm{matrix}}$; $V=V_0$). Eigenenergies and eigenfunctions for the confined particle in the quantum dot can be found by direct diagonalization of the Hamiltonian matrix H_0. In III-V semiconductors, V_0 represents the conduction-band and valence-band offsets and are well known. On the other hand, for 6H-SiC nanocrystals surrounded by a solvent (ethanol, water,…), these offsets are not well known. So, in our calculations, we have considered the values of $V_0=10$ eV (almost infinite barrier) for the conduction band as well as for the valence band. It should be noted here that we took account of the dielectric constant of the solvent (in this case ethanol) which is different from the 6H-SiC nanoparticles one. We thus determine the transition energies as the eigenvalues of the Hamiltonian which describes the electron-hole pair. The nanoparticle size has been adjusted in order to fit the experimental values. Best fit was obtained considering a 1.9 nm diameter. The results are given in Table I and compared with the values of the threshold values of the peaks determined in Fig. 4. As one can see, a good agreement between calculated and experimentally deduced values is found (especially in the case of the fundamental level). The discrepancies are more important for the excited levels. This can be explained by the fact that the determination of these values is more sensitive to the estimated value of V_0, i.e., a wrong estimation of V_0 implies a greater error on the determination of the excited levels compared to that of the fundamental level. Nevertheless, the assumed value of V_0 (i.e, 10 eV) yields a good general agreement between experimental and calculated values confirming thus the global validity of our assumptions.

IV. CONCLUSIONS

To conclude, we have shown that the luminescence mechanisms governing the intense room-temperature PL of the 6H-SiC nanostructures (porous layer, nanopowder, and colloidal suspension) formed by electrochemical etching can be efficiently selected by controlling their surface chemical environment and their dimensions. In particular, PL of dry 6H-SiC nanoparticles is mainly driven by radiative transitions between electronically active surface states. Nonradiative and radiative surface states controlling the PL emission of the dry nanopowder can be efficiently screened by a polar wetting medium such as ethanol, for example. Working with colloidal suspensions of the nanoparticles allowed us to perform size selection of the nanoparticles by the use of centrifugation. Centrifugation induces selection of the smallest 6H-SiC nanocrystals (<2 nm in diameter) in which probability to have both donor and acceptor atoms is negligible. Radiative transitions between these impurity levels are thus avoided. For these smallest 6H-SiC nanocrystals with switched off transitions via surface states and via impurity levels, the quantum confinement is manifested by above-gap photoluminescence and observation of energy subbands in absorption measurement.

While a long controversy has gripped the scientific community about the photoluminescence origin in Si nanostructures (surface related vs quantum confinement), we show from these first results on 6H SiC nanocrystals that these two radiative channels plus impurity levels transitions are present and that one has to suppress surface states and impurity-related mechanisms in order to observe transitions from the confined carriers in the quantum dots.

ACKNOWLEDGMENTS

This work was partially supported by INSA de Lyon within the frame of a BQR-2006 research grant. The authors acknowledge Y. Chevolot from Ecole Centrale de Lyon for his helpful technical support with the absorption measurements.

[1] T. Matsumoto, J. Takahashi, T. Tamaki, T. Futagi, H. Mimura, and Y. Kanemitsu, Appl. Phys. Lett. **64**, 226 (1994).
[2] A. O. Konstantinov, A. Henry, C. I. Harris, and E. Janzén, Appl. Phys. Lett. **66**, 2250 (1995).
[3] O. Jessensky, F. Müller, and U. Gösele, Thin Solid Films **297**, 224 (1997).
[4] T. L. Rittenhouse, P. W. Bohn, T. K. Hoossain, I. Adesida, J. Lindesay, and A. Marcus, J. Appl. Phys. **95**, 490 (2004).
[5] V. Petrova-Koch, O. Sreseli, G. Polisski, D. Kovalev, T. Muschik, and F. Koch, Thin Solid Films **255**, 107 (1995).
[6] R. P. Devaty and W. J. Choyke, Phys. Status Solidi A **162**, 5 (1997).
[7] X. L. Wu, J. Y. Fan, T. Qiu, X. Yang, G. G. Siu, and P. K. Chu, Phys. Rev. Lett. **94**, 026102 (2005).
[8] J. Y. Fan, X. L. Wu, H. X. Li, H. W. Liu, G. G. Siu, and P. K. Chu, Appl. Phys. Lett. **88**, 041909 (2006).
[9] J. Y. Fan, X. L. Wu, and P. K. Chu, Prog. Mater. Sci. **51**, 983 (2006).

[10] S. Alekseev, V. Zaitsev, J. Botsoa, and D. Barbier, Chem. Mater. **19**, 2189 (2007).
[11] S. H. Hagen, A. W. C. Van Kemenade, and J. A. W. Van Der Does De Bye, J. Lumin. **8**, 18 (1973).
[12] J. Botsoa, J.-M. Bluet, V. Lysenko, and G. Guillot, J. Appl. Phys. **102**, 083526 (2007).
[13] J.-N. Chazalviel, F. Ozanam and V. M. Dubin, J. Phys. I **4**, 1325 (1994).
[14] H. A. Lopez, X. N. Chen, S. A. Jenekhe, and P. M. Fauchet, J. Lumin. **80**, 115 (1999).
[15] V. Yu. Timoshenko, Th. Dittrich, V. Lysenko, M. G. Lisachenko, and F. Koch, Phys. Rev. B **64**, 085314 (2001).
[16] A. Franceschetti and S. T. Pantelides, Phys. Rev. B **68**, 033313 (2003).
[17] T. Qiu, X. L. Wu, F. Kong, H. B. Ma, and Paul K. Chu, Phys. Lett. A **334**, 447 (2005).
[18] J. E. Brus, J. Chem. Phys. **80**, 4403 (1984).
[19] M. Baira, L. Sfaxi, L. Bouzaiene, H. Maaref, N. Chauvin, and C. Bru-Chevallier, J. Appl. Phys. **104**, 064314 (2008).